Journal of Solid Mechanics Vol. 12, No. 4 (2020) pp. 752-773

Refined Zigzag Theory for Nonlinear Dynamic Response of an Axially Moving Sandwich Nano beam Embedded on Visco-Pasternak Medium Using MCST

A. Ghorbanpour Arani [1,2 *], M. Abdollahian[1]

[1]*Faculty of Mechanical Engineering, University of Kashan, Kashan, Islamic Republic of Iran*
[2]*Institute of Nanoscience & Nanotechnology, University of Kashan, Kashan, Islamic Republic of Iran*

Received 5 July 2020; accepted 8 September 2020

ABSTRACT

This paper develops the Refined Zigzag Theory (RZT) for nonlinear dynamic response of an axially moving functionally graded (FG) Nano beam integrated with two magnetostrictive face layers based on the modified couple stress theory (MCST). The Sandwich Nano beam (SNB) subjected to a temperature difference and both axial and transverse mechanical loads. The material properties of FG core layer depend on the environment temperature and are assumed to vary in thickness direction. The SNB is surrounded by elastic medium, which is simulated by visco-Pasternak model. The von-Karman nonlinear strain-displacement relationships are employed to consider the effect of geometric nonlinearities. In order to obtain governing motion equations and boundary conditions the energy method as well as Hamilton's principle is applied. The differential quadrature method (DQM) is used for space domain and the Newmark-β method is taken into account for time domain response of the axially moving SNB. The detailed parametric study is conducted to investigate the effects of surrounding elastic medium, material length scale parameter, magnetostrictive layers, temperature difference, environment temperature, velocity of the SNB, axial and transverse mechanical loads and volume fraction exponent on the dynamic response of the SNB. Results indicate that the maximum deflection of the system can be controlled by employing negative values of velocity feedback gain values. In addition, the system loses its stability when the velocity of SNB is increased.

Keywords: Nonlinear dynamic response; Magnetostrictive; Axially moving Nano beam; Visco-Pasternak; Refined zigzag theory.

1 INTRODUCTION

SANDWICH beams are one of the most important of sandwich structures, which consists of two relatively thin

*Corresponding author. Tel.: +98 31 5591 2450; Fax: +98 31 5591 2424.
E-mail address: aghorban@kashanu.ac.ir (A. Ghorbanpour Arani).

and stiff faces at bottom, and top that perfectly bonded to a thick lightweight core. In fact, the face sheets have enough stiffness and strength while the core layer chosen from lightweight and stiff materials. Due to this fact, they can be used in many engineering structures especially in aircrafts, space vehicles, automobile, electronics and others [1-7]. In order to analyze the mechanical response of sandwich beams different theories such as layer-wised theories (LW) and also equivalent single-layer theories (ESL), which contains classical laminate theory (CLT) and first order shear deformation theory can be applied. Among the mentioned models, CLT yields inaccurate results in compare with other theories since it neglects the shear strains and stresses. On the other hand, the weakness point of the FSDT is that its results depend on the shear correction factor. To solve the problem of FSDT, higher order beam theories (HOBTs) have been introduced and implemented by many researchers [8-11]. Akgoz and Civalek [8] employed a trigonometric shear deformation beam model to investigate the mechanical responses of isolated microtubules and included that effects of shear deformation become more significant for smaller shear modulus and aspect ratios. HOBT including non-linear distribution of shear stress through thickness of laminated beam was presented by Ozutok and Madenci [9] to analyze the static behavior of laminated composite beams. Shao et al. [10] presented a unified formulation which was based on a general refined shear deformation beam theory to conduct free vibration analysis of composite laminated beams subjected to general boundary conditions. Zhang and Taheri [11] simulated the dynamic pulsebuckling and postbuckling response of fiber-reinforced (FRP) laminated beams using higher order shear deformation theory. Although using HOBTs solve the problem of using other ESL theories such as CLT and FSDT, but generally ESL theories predicts inaccurate results for thick and especially sandwich beams. Therefore, using LW theories can be one of the choice of researchers. But the problem of employing LW theories for sandwich structures is that even though, LW theories are more accurate than ESL theories, they are not suitable especially for multilayered structures since the numbers of unknowns are proportional to the number of layers [12]. However, since in zigzag (ZZ) theories the number of unknowns are regardless of the layers number and also these theories are more computationally efficient than ESL and LW theories, ZZ theories can be chosen as a good choice to analyze the mechanical responses of sandwich structures. Due to this fact that many ZZ theories requires C1 continuity Tessler et al. [13, 14] presented a modified ZZ model known as RZT which needs C0 continuous interpolation for all the kinematic variables [15]. Si Sciuva et al. [16] formulated a class of efficient higher-order C0-continuous beam elements based on RZT. The RZT was presented for laminated-composite and sandwich plates by Tessler et al. [17]. In another attempt, based on RZT, Gherlone et al. [18] analyzed the multilayered composite and sandwich beams. Analyzing the mechanical responses of nanostructures using conventional elasticity theory predicts inaccurate results since the effect of material length scale parameter have not been taken into account. To overcome this problem several non-classical theories have been introduced such as nonlocal elasticity theory [19-25], surface elasticity theory [26], MCST [27-31] and modified strain gradient theory [32-36]. Among mentioned theories, since MCST predicts accurate results in addition to less computational efforts, it can be selected as an appropriate theory to analyze the mechanical behavior of micro and nano structures. Therefore, many researchers have been applied MCST to capture the size effects. For instance, Ke and Wang [28] investigated the dynamic stability of micro beams made of functionally gadded materials (FGMs) based on the MCST and TB model and showed that the size effect on the dynamic stability characteristics is significant only when the thickness of beam has a similar value to the material length scale parameter. In another attempt, they [29] investigated vibration and instability of fluid-conveying double-walled carbon nanotubes (DWCNTs) based on MCST. They concluded that the imaginary component of the frequency and the critical flow velocity the fluid-conveying DWCNTs increase with increase in the length scale parameter. Based on the modified couple stress theory the nonlinear resonant dynamic of a microscale beam was studied numerically by Ghayesh et al. [31]. Most of the time in real applications, the structure surrounded by an elastic medium. The surrounded foundation can be simulated by different assumptions depend on the forces applied to the structure from the media. For instance the Winkler type of elastic medium considers only the normal forces of elastic medium. In comparison to the Winkler type model, the Pasternak elastic medium which considers both shear and normal forces are more accurate and it is sufficient for researchers to use this model as the surrounded elastic foundation. Ghorbanpour Arani et al. [32] studied the nonlinear vibration of a Nano beam elastically connected to a piezoelectric Nano beam using Pasternak foundation. Amir et al. [37] investigated the buckling analysis of nanocomposite sandwich plates with piezoelectric face sheets rested on Pasternak foundation based on flexoelectricity and first-order shear deformation theories. In another attempt, Amir et al. [38] studied the size-dependent vibration analysis of a three-layered porous rectangular nano plate with piezo-electromagnetic face sheets subjected to pre loads based on SSDT. Lee and Jeong [39] developed the out-of-plane free vibrations of curved beams with variable curvature on a Pasternak foundation. Sobamowo [40] presented analytical solutions using differential transformation method with after-treatment technique for nonlinear analysis of thermal and flow-induced vibration of fluid-conveying carbon nanotube resting on Winkler and Pasternak foundations. Ghorbanpour Arani et al. [41] analyzed the electro-thermo-torsional buckling of a double-walled boron

nitride nanotube embedded on Pasternak elastic medium. Their results showed that increasing the shear modulus of Pasternak foundation increases the buckling load. The weakness of Pasternak simulation is neglecting damping effects of elastic medium, which may yields inaccurate results. Therefore, many researchers have been employed visco-Pasternak elastic medium in their analysis. For instance, the general equation for transverse vibration of double-viscoelastic-FGM-nanoplate system with viscoelastic Pasternak medium was formulated by Liu et al. [42]. Mohammadi et al. [43] studied the vibration behavior of the rotating viscoelastic Nano beam embedded in the visco-Pasternak foundation. An analytical process was proposed by Jamalpoor et al. [44] to investigate the size-dependent free vibration of orthotropic multi-viscoelastic microplate systems embedded in Kelvin-Voigt visco-Pasternak medium based on the modified strain gradient theory. Magnetostrictive materials can be applied as smart materials, since they undergo deformation when subjected to magnetic field and vice versa. Motivated by these considerations, magnetostrictive materials have received plenty of attentions and many researchers have been studied the mechanical response of these materials. Hong [45] used generalized differential quadrature (GDQ) method to compute the transient response of thermal stresses and center displacement in laminated magnetostrictive plates. In another attempt, Hong [46] investigated thermal vibration and transient response of FGM plate with mounted magnetostrictive layer using GDQ method. Ghorbanpour Arani and Abdollahian [47] studied the transient response of a FG Nano beam integrated with magnetostrictive layers embedded on visco-Pasternak elastic foundation. Analytical solutions of FGM shells with embedded magnetostrictive layers were presented by Pradhan [48]. The problem of dynamic response of axially moving beams has received plenty of attentions, since axially moving beams are used in various engineering applications such as robotic manipulators, telescopic members of loading vehicles and machine tools [49]. Ghayesh and Amabili [50] investigated the non-linear dynamics of an axially moving beam with time-dependent axial speed, including numerical results for the non-linear resonant response of the system in the sub-critical speed regime and global dynamical behavior. Lim et al. [51] studied the transverse free vibrations of axially moving Nano beams subjected to axial tension based on nonlocal stress elasticity theory. They discussed the influences of nonlocal nanoscale and axial tension on the critical velocity. Applying the nonlocal theory and considering small fluctuations in the axial velocity, the stability and non-linear vibrations of an axially moving nanoscale visco-elastic Rayleigh beam were studied by Rezaee and Lotfan [52]. In another attempt, Ghorbanpour Arani et al. [53] investigated vibration and instability of axially moving single-layered grapheme sheet (SLGS) embedded on visco-Pasternak foundation. They concluded that the critical speed of moving SLGS can be improved by applying magnetic field.

However, no report has been found in the literature on the nonlinear dynamic response of axially moving SNBs so far. Motivated by these considerations in the present manuscript, applying the von-Karman nonlinear strain-displacement relationships, transient response of an axially moving FG core integrated with magnetostrictive layers subjected to thermal and mechanical loads is studied using RZT. The MSCT has been employed to capture the effect of small scale parameter. The SNB is surrounded by an elastic medium, which is simulated by visco-Pasternak model. Using DQM for space domain in conjunction with the Newmark- β method for time domain the results are obtained which are then presented graphically to depicts the influences of material length scale parameter, Visco-Pasternak elastic medium, magnetostrictive layers, environment and difference temperature, velocity of the SNB, applied mechanical forces and volume fraction exponent. The results of the present study can be used in designing nano electro mechanical systems (NEMS) especially where the magnetostrictive materials have been used.

2 MODIFIED COUPLE STRESS THEORY

The strain energy derived from the MCST is expressed as function of the symmetric strain tensor ε_{ij} and the symmetric rotation gradient tensor χ_{ij} . Therefore, for a linear elastic material occupying region V with infinitesimal deformations the strain energy Π_s is written a follows [27-31]:

$$\Pi_s = \frac{1}{2}\int_V \left(\sigma_{ij}^{(k)}\varepsilon_{ij}^{(k)} + m_{ij}^{(k)}\chi_{ij}^{(k)}\right)dV \,,\left(i\,,j=x\,,y\,,z\right), \tag{1}$$

where σ_{ij} is the Cauchy stress and m_{ij} is the deviatoric part of the couple stress tensor and:

$$\varepsilon_{ij}^{(k)}=\frac{1}{2}\left(u_{i,j}^{(k)}+u_{j,i}^{(k)}+u_{m,i}^{(k)}u_{m,j}^{(k)}\right), \tag{2a}$$

$$\chi_{ij}^{(k)}=\frac{1}{2}\left(\theta_{i,j}^{(k)}+\theta_{j,i}^{(k)}\right), \tag{2b}$$

$$\theta_{i}^{(k)}=\frac{1}{2}e_{ijn}u_{n,j}^{(k)}, \tag{2c}$$

In which u_i , θ_i and e_{ijk} are the displacement vector, the infinitesimal rotation vector and the alternate tensor, respectively.

3 PRELIMINARIES BASED ON RZT

Schematically representation of the axially moving SNB with rectangular cross section with total thickness h_l , width b and length L is shown in Fig. 1. The Cartesian coordinate system (x,y,z) is taken as a reference where the longitudinal axis x varies from 0 to L, the thickness coordinate z ranges from $-h_l/2$ to $h_l/2$, and the width coordinate y changes from $-b/2$ to $b/2$. The core thickness is h_c and the integer (k) changes from 1 to 3, indicates the number of each layer from the bottom to the top of the SNB and the cross sectional area of each layer is A_k . The Nano beam is subjected to temperature difference and axial and transverse mechanical loads. Furthermore, it is assumed that the SNB surrounded by visco-Pasternak elastic medium.

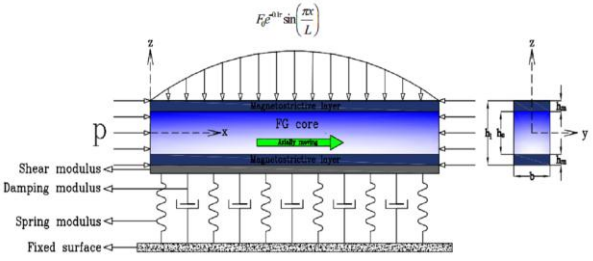

Fig.1
Schematic of an axially moving SNB embedded on visco-Pasternak medium.

Based on the RZT the nonzero displacement components of an arbitrary point of the SNB $u_x^{(k)}(x,z,t)$ and $u_z^{(k)}(x,z,t)$ in the x and z directions, respectively, can be written as follows: [18]:

$$u_x^{(k)}(x,z,t)=u(x,t)+z\theta(x,t)+\Phi^{(k)}(z)\psi(x,t), \tag{3a}$$

$$u_z^{(k)}(x,z,t)=w(x,t), \tag{3b}$$

where $u(x,t)$ and $w(x,t)$ are the in-plane displacements in the x and z directions, respectively; $\theta(x,t)$, $\psi(x,t)$ and $\Phi^{(k)}(z)$ are the average cross-sectional rotation, the amplitude of zigzag rotation and the zigzag function, respectively. The zigzag function can be obtained from the following relations as [17]:

$$\Phi^{(1)}=\left(z+\frac{h_l}{2}\right)\left(\frac{G_1}{Q_{11}^{(1)}}-1\right), \tag{4a}$$

$$\Phi^{(q)}=\left(z+\frac{h_l}{2}\right)\left(\frac{G_1}{Q_{11}^{(q)}}-1\right)+\sum_{p=2}^{3}h^{(p-1)}\left(\frac{G_1}{Q_{11}^{(p-1)}}-\frac{G_1}{Q_{11}^{(q)}}\right)(q=2,3), \tag{4b}$$

In which:

$$G_1=\left(\frac{2}{h_l}\sum_{k=1}^{3}\frac{h^{(k)}}{Q_{11}^{(k)}}\right)^{-1}, \tag{5}$$

where $Q_{lm}^{(k)}(l,m=1,\ldots,6)$ and $h^{(k)}$ are the elastic constant and thickness of *kth* layer, respectively.

Inserting Eqs. (3) into Eq. (2c) yields the components of rotations as follows:

$$\theta_x^{(k)}=0, \tag{6a}$$

$$\theta_y^{(k)}=\frac{1}{2}\left(\theta+\frac{d\Phi^{(k)}(z)}{dz}\psi-\frac{\partial w}{\partial x}\right), \tag{6b}$$

$$\theta_z^{(k)}=0. \tag{6c}$$

Substituting Eqs. (3) into Eqs. (2a) results the von-Karman nonlinear strain-displacement relationships as follows:

$$\varepsilon_{xx}^{(k)}=\frac{\partial u}{\partial x}+z\frac{\partial\theta}{\partial x}+\frac{1}{2}\left(\frac{\partial w}{\partial x}\right)^2+\Phi^{(k)}(z)\frac{\partial\psi}{\partial x}, \tag{7a}$$

$$\gamma_{xz}^{(k)}=2\varepsilon_{xz}^{(k)}=\theta+\frac{d\Phi^{(k)}(z)}{dz}\psi+\frac{\partial w}{\partial x}. \tag{7b}$$

Using Eqs. (3) into Eqs. (2b) the components of the symmetric rotation gradient tensor are obtained as:

$$\chi_{xy}^{(k)}=\frac{1}{4}\left(\frac{\partial\theta}{\partial x}+\frac{d\Phi^{(k)}(z)}{dz}\frac{\partial\psi}{\partial x}-\frac{\partial^2 w}{\partial x^2}\right), \tag{8a}$$

$$\chi_{yz}^{(k)}=\frac{1}{4}\frac{d^2\Phi^{(k)}(z)}{dz^2}\psi. \tag{8b}$$

4 ENERGY METHOD

4.1 Strain energy

Substituting Eqs. (7) and (8) into Eq. (1) yields the total strain energy of the SNB as follows:

$$\Pi_s=\frac{1}{2}\int_0^L\left(N_x\left(\frac{\partial u}{\partial x}+\frac{1}{2}\left(\frac{\partial w}{\partial x}\right)^2\right)+M_x\frac{\partial\theta}{\partial x}+M_\Phi\frac{\partial\psi}{\partial x}+Q_x\left(\theta+\frac{\partial w}{\partial x}\right)+Q_\Phi\psi+\frac{Y_1}{2}\left(\frac{\partial\theta}{\partial x}-\frac{\partial^2 w}{\partial x^2}\right)\right.$$
$$\left.+\frac{Y_2}{2}\frac{\partial\psi}{\partial x}+\frac{Y_3}{2}\psi\right)dx, \tag{9}$$

where:

$$\left(N_x, M_x, M_\Phi\right)=\sum_{k=1}^{3}\int_{A_k}\sigma_{xx}^{(k)}\left\{1, z, \Phi^{(k)}(z)\right\}dA_k, \left(Q_x, Q_\Phi\right)=\sum_{k=1}^{3}\int_{A_k}\sigma_{xz}^{(k)}\left\{1, \frac{d\Phi^{(k)}(z)}{dz}\right\}dA_k,$$
$$\left(Y_1, Y_2\right)=\sum_{k=1}^{3}\int_{A_k} m_{xy}^{(k)}\left\{1, \frac{d\Phi^{(k)}(z)}{dz}\right\}dA_k, Y_3=\sum_{k=1}^{3}\int_{A_k} m_{yz}^{(k)}\frac{d^2\Phi(z)}{dz^2}dA_k. \tag{10}$$

4.2 Kinetic energy

The kinetic energy of the axially moving SNB is calculated from the following relation as [53]:

$$\Pi_k=\frac{1}{2}\sum_{k=1}^{3}\int_0^L\int_{A_k}\rho^{(k)}(z)\left[\left(V_x+\frac{\partial u_x^{(k)}}{\partial t}+V_x\frac{\partial u_x^{(k)}}{\partial x}\right)^2+\left(\frac{\partial u_z^{(k)}}{\partial t}+V_x\frac{\partial u_z^{(k)}}{\partial x}\right)^2\right], \tag{11}$$

In which $\rho^{(k)}$ is the density of *k th* layer and V_x denotes the velocity of the SNB. Eq. (11) can be rewritten by substituting Eqs. (3) Into Eq. (11) as follows:

$$\begin{aligned}\Pi_k=&\frac{1}{2}\sum_{k=1}^{3}\int_0^L\int_{A_k}\left[I_A\left(V_x+\frac{\partial u}{\partial t}+V_x\frac{\partial u}{\partial x}\right)^2+I_D\left(\frac{\partial\theta}{\partial t}+V_x\frac{\partial\theta}{\partial x}\right)^2+I_H\left(\frac{\partial\psi}{\partial t}+V_x\frac{\partial\psi}{\partial x}\right)^2\right.\\&+2I_B\left(V_x+\frac{\partial u}{\partial t}+V_x\frac{\partial u}{\partial x}\right)\left(\frac{\partial\theta}{\partial t}+V_x\frac{\partial\theta}{\partial x}\right)+2I_E\left(V_x+\frac{\partial u}{\partial t}+V_x\frac{\partial u}{\partial x}\right)\left(\frac{\partial\psi}{\partial t}+V_x\frac{\partial\psi}{\partial x}\right)\\&\left.+2I_F\left(\frac{\partial\theta}{\partial t}+V_x\frac{\partial\theta}{\partial x}\right)\left(\frac{\partial\psi}{\partial t}+V_x\frac{\partial\psi}{\partial x}\right)+I_A\left(\frac{\partial w}{\partial t}+V_x\frac{\partial w}{\partial x}\right)^2\right],\end{aligned} \tag{12}$$

where:

$$\left(I_A, I_B, I_D\right)=\sum_{k=1}^{3}\int_{A_k}\rho^{(k)}(z)\left(1, z, z^2\right)dA_k,$$
$$\left(I_E, I_F, I_H\right)=\sum_{k=1}^{3}\int_{A_k}\rho^{(k)}(z)\Phi^{(k)}(z)\left(1, z, \Phi^{(k)}(z)\right)dA_k. \tag{13}$$

4.3 External forces

To calculate the virtual work the axial force *p*, visco-Pasternak foundation F_e and distributed transverse load $f(x,t)$ should be taken into consideration.

The force induced by the elastic medium can be expressed as [47]:

$$F_e=-k_w w+k_g\frac{\partial^2 w}{\partial x^2}-k_c\frac{\partial w}{\partial t}, \tag{14}$$

where k_w, k_g and k_c are spring, shear and damping modulus, respectively. Also, the distributed transverse load can be written as follows:

$$f(x,t)=f_0F(x)G(t), \tag{15}$$

In which f_0 is a constant and the functions $F(x)$ and $G(t)$ depend on the externally distributed load. Therefore, the first variation of the external applied forces W_{ext} can be given as:

$$\begin{aligned}\delta W_{ext} &= \int_0^L \left(-k_w w\,\delta w - k_g \frac{\partial w}{\partial x}\frac{\partial \delta w}{\partial x} - k_c \frac{\partial w}{\partial t}\delta w + P\frac{\partial \delta u}{\partial x} + P\frac{\partial w}{\partial x}\frac{\partial \delta w}{\partial x} + f\,\delta w \right) dx \\ &= -\int_0^L k_w w\,\delta w dx - k_g \frac{\partial w}{\partial x}\delta w\Big|_0^L + \int_0^L k_g \frac{\partial^2 w}{\partial x^2}\delta w dx - \int_0^L k_c \frac{\partial w}{\partial t}\delta w dx + p\delta u\Big|_0^L + P\frac{\partial w}{\partial x}\delta w\Big|_0^L \\ &\quad -\int_0^L P\frac{\partial^2 w}{\partial x^2}\delta w dx + \int_0^L f\,\delta w dx .\end{aligned} \tag{16}$$

5 HAMILTON'S PRINCIPLE

The governing motions equations and boundary conditions can be obtained using Hamilton's principle as follows [18]:

$$\delta \int_0^T \left(\Pi_k - \Pi_s + W_{ext} \right) dt = 0, \tag{17}$$

Inserting Eqs. (9), (12) and (16) into Eq. (17), after some mathematical manipulations, the governing motion equations of SNB are obtained as:

$$\begin{aligned}&\delta u : \frac{\partial N_x}{\partial x} = I_A \frac{\partial^2 u}{\partial t^2} + 2I_A V_x \frac{\partial^2 u}{\partial t\,\partial x} + I_A V_x^2 \frac{\partial^2 u}{\partial x^2} + I_B \frac{\partial^2 \theta}{\partial t^2} + 2I_B V_x \frac{\partial^2 \theta}{\partial t\,\partial x} + I_B V_x^2 \frac{\partial^2 \theta}{\partial x^2} + I_E \frac{\partial^2 \psi}{\partial t^2} \\ &+2I_E V_x \frac{\partial^2 \psi}{\partial t\,\partial x} + I_E V_x^2 \frac{\partial^2 \psi}{\partial x^2},\end{aligned} \tag{18a}$$

$$\begin{aligned}&\delta w : \frac{\partial}{\partial x}\left(N_x \frac{\partial w}{\partial x} \right) + \frac{\partial Q_x}{\partial x} + \frac{1}{2}\frac{\partial^2 Y_1}{\partial x^2} - k_w w + k_g \frac{\partial^2 w}{\partial x^2} - k_c \frac{\partial w}{\partial t} - p\frac{\partial^2 w}{\partial x^2} + f = I_A \frac{\partial^2 w}{\partial t^2} \\ &+2I_A V_x \frac{\partial^2 w}{\partial t\,\partial x} + I_A V_x^2 \frac{\partial^2 w}{\partial x^2},\end{aligned} \tag{18b}$$

$$\begin{aligned}&\delta \theta : \frac{\partial M_x}{\partial x} - Q_x + \frac{1}{2}\frac{\partial Y_1}{\partial x} = I_D \frac{\partial^2 \theta}{\partial t^2} + 2I_D V_x \frac{\partial^2 \theta}{\partial t\,\partial x} + I_D V_x^2 \frac{\partial^2 \theta}{\partial x^2} + I_B \frac{\partial^2 u}{\partial t^2} + 2I_B V_x \frac{\partial^2 u}{\partial t\,\partial x} \\ &+I_B V_x^2 \frac{\partial^2 u}{\partial x^2} + I_F \frac{\partial^2 \psi}{\partial t^2} + 2I_F V_x \frac{\partial^2 \psi}{\partial t\,\partial x} + I_F V_x^2 \frac{\partial^2 \psi}{\partial x^2},\end{aligned} \tag{18c}$$

$$\begin{aligned}&\delta \psi : \frac{\partial M_\Phi}{\partial x} - Q_\Phi + \frac{1}{2}\frac{\partial Y_2}{\partial x} - \frac{Y_3}{2} = I_H \frac{\partial^2 \psi}{\partial t^2} + 2I_H V_x \frac{\partial^2 \psi}{\partial t\,\partial x} + I_H V_x^2 \frac{\partial^2 \psi}{\partial x^2} + I_E \frac{\partial^2 u}{\partial t^2} + 2I_E V_x \frac{\partial^2 u}{\partial t\,\partial x} \\ &+I_E V_x^2 \frac{\partial^2 u}{\partial x^2} + I_F \frac{\partial^2 \theta}{\partial t^2} + 2I_F V_x \frac{\partial^2 \theta}{\partial t\,\partial x} + I_F V_x^2 \frac{\partial^2 \theta}{\partial x^2}.\end{aligned} \tag{18d}$$

Moreover, the related boundary conditions are obtained as follows:

$$\begin{aligned}&t = 0, T: \ u = 0 \ \ or \ \ I_A V_x + I_A \frac{\partial u}{\partial t} + I_A V_x \frac{\partial u}{\partial x} + I_B \frac{\partial \theta}{\partial t} + I_B V_x \frac{\partial \theta}{\partial t} + I_E \frac{\partial \psi}{\partial t} + I_E V_x \frac{\partial \psi}{\partial t} = 0, \\ &x = 0, L: \ u = 0 \ \ or \ \ I_A V_x^2 + I_A V_x \frac{\partial u}{\partial t} + I_A V_x^2 \frac{\partial u}{\partial x} + I_B V_x \frac{\partial \theta}{\partial t} + I_B V_x^2 \frac{\partial \theta}{\partial x} + I_E V_x \frac{\partial \psi}{\partial t} + I_E V_x^2 \frac{\partial \psi}{\partial x} - N_x + p = 0,\end{aligned} \tag{19a}$$

$$t=0,T:\ w=0\quad or\quad I_A\frac{\partial w}{\partial t}+I_AV_x\frac{\partial w}{\partial x}=0,$$
$$x=0,L:\ w=0\quad or\quad I_AV_x\frac{\partial w}{\partial t}+I_AV_x^2\frac{\partial w}{\partial x}-N_x\frac{\partial w}{\partial x}-Q_x-\frac{1}{2}\frac{\partial Y_1}{\partial x}+p\frac{\partial w}{\partial x}-k_g\frac{\partial w}{\partial x}=0, \tag{19b}$$

$$x=0,L:\ \frac{\partial w}{\partial x}=0,\ or\ \frac{Y_1}{2}=0, \tag{19c}$$

$$t=0,T:\ \theta=0\quad or\quad I_D\frac{\partial \theta}{\partial t}+I_DV_x\frac{\partial \theta}{\partial x}+I_BV_x+I_B\frac{\partial u}{\partial t}+I_BV_x\frac{\partial u}{\partial x}+I_F\frac{\partial \psi}{\partial t}+I_FV_x\frac{\partial \psi}{\partial x}=0,$$
$$x=0,L:\ \theta=0\quad or\quad I_DV_x\frac{\partial \theta}{\partial t}+I_DV_x^2\frac{\partial \theta}{\partial x}+I_BV_x^2+I_BV_x\frac{\partial u}{\partial t}+I_BV_x^2\frac{\partial u}{\partial x}+I_FV_x\frac{\partial \psi}{\partial t}$$
$$+I_FV_x^2\frac{\partial \psi}{\partial x}-M_x-\frac{Y_1}{2}=0, \tag{19d}$$

$$t=0,T:\ \psi=0\quad or\quad I_H\frac{\partial \psi}{\partial t}+I_HV_x\frac{\partial \psi}{\partial x}+I_EV_x+I_E\frac{\partial u}{\partial t}+I_EV_x\frac{\partial u}{\partial x}+I_F\frac{\partial \theta}{\partial t}+I_FV_x\frac{\partial \theta}{\partial x}=0,$$
$$x=0,L:\ \psi=0\quad or\quad I_HV_x\frac{\partial \psi}{\partial t}+I_HV_x^2\frac{\partial \psi}{\partial x}+I_EV_x^2+I_EV_x\frac{\partial u}{\partial t}+I_EV_x^2\frac{\partial u}{\partial x}+I_FV_x\frac{\partial \theta}{\partial t}$$
$$+I_FV_x^2\frac{\partial \theta}{\partial x}-M_\Phi-\frac{1}{2}Y_2=0. \tag{19e}$$

In order to find the governing motion equations and boundary conditions in terms of displacements, it is necessary to introduce the nonzero stress components and deviatoric part of the couple stress for FG core and magnetostrictive layers of SNB as [46, 54]:

$$\sigma_{xx}^{(2)}=Q_{11}^{(2)}\varepsilon_{xx}^{(2)}-\alpha_x^{(2)}\Delta T, \tag{20a}$$

$$\sigma_{xz}^{(2)}=Q_{55}^{(2)}\gamma_{xz}^{(2)}, \tag{20b}$$

$$\sigma_{xx}^{(1,3)}=Q_{11}^{(1,3)}\varepsilon_{xx}^{(1,3)}-e_{31}^{(1,3)}H_z-\alpha_x^{(1,3)}\Delta T, \tag{20c}$$

$$\sigma_{xz}^{(1,3)}=Q_{55}^{(1,3)}\gamma_{xx}^{(1,3)}, \tag{20d}$$

$$m_{xy}^{(k)}=2Q_{55}^{(k)}l^2\chi_{xy}^{(k)}, \tag{20e}$$

$$m_{yz}^{(k)}=2Q_{55}^{(k)}l^2\chi_{yz}^{(k)}, \tag{20f}$$

where $e_{31}^{(1,3)}$ is the magnetostrictive material coefficient, l is the material length scale parameter, ΔT indicates the temperature difference, $\alpha_x^{(k)}$ is the longitudinal thermal expansion coefficient of *k th* layer and:

$$Q_{11}^{(2)}=\frac{E(z)}{1-\nu(z)^2},Q_{55}^{(2)}=\frac{E(z)}{2(1+\nu(z))}, \tag{21a}$$

$$H_z=k_cc(t)\frac{\partial w}{\partial t}, \tag{21b}$$

where k_c is the coil constant and $c(t)$ denotes the control gain [45-48]; Moreover, the Young's modulus E, Poisson's ratio v and density ρ_c of the FGM core can be expressed as [47, 48]:

$$E = (E_2 - E_1)\left(\frac{2z + h_c}{2h_c}\right)^{\gamma} + E_1, \tag{22a}$$

$$\nu = (\nu_2 - \nu_1)\left(\frac{2z + h_c}{2h_c}\right)^{\gamma} + \nu_1, \tag{22b}$$

$$\rho_c = (\rho_{c2} - \rho_{c1})\left(\frac{2z + h_c}{2h_c}\right)^{\gamma} + \rho_{c1}, \tag{22c}$$

where E_2 and E_1 are the Young's moduli, ν_2 and ν_1 are the Poisson's ratio, ρ_{c2} and ρ_{c1} are the density of the constituent materials and γ is the volume fraction exponent, respectively [47, 48].

On the other hand, due to this fact that most of FGM are used in high temperature applications, each property of the SNB core layer Z depends on the environment temperature $T(K)$ as follows [47, 48]:

$$Z = Z_0\left(Z_{-1}T^{-1} + 1 + Z_1T^1 + Z_2T^2 + Z_3T^3\right), \tag{23}$$

where Z_0, Z_{-1}, Z_1, Z_2 and Z_3 are temperature coefficients of the constituent materials.

Substituting Eq. (20) into Eq. (10), and then using the obtained relations in Eqs. (18) and (19) the governing motion equations and boundary conditions are obtained in terms of displacement components as follows:

$$\begin{aligned}&\frac{\partial^2 U}{\partial X^2} + \bar{B}_{11}\frac{\partial^2 \Theta}{\partial X^2} + \eta\frac{\partial W}{\partial X}\frac{\partial^2 W}{\partial X^2} + \bar{E}_{11}\frac{\partial^2 \Psi}{\partial X^2} - M_{31}\frac{\partial^2 W}{\partial X\,\partial \tau} - 2\bar{V}_x\frac{\partial^2 U}{\partial \tau \partial X} - \bar{V}_x^2\frac{\partial^2 U}{\partial X^2}\\ &-2\bar{I}_B\bar{V}_x\frac{\partial^2 \Theta}{\partial \tau \partial X} - \bar{I}_B\bar{V}_x^2\frac{\partial^2 \Theta}{\partial X^2} - 2\bar{I}_E\bar{V}_x\frac{\partial^2 \Psi}{\partial \tau \partial X} - \bar{I}_E\bar{V}_x^2\frac{\partial^2 \Psi}{\partial X^2} = \frac{\partial^2 U}{\partial \tau^2} + \bar{I}_B\frac{\partial^2 \Theta}{\partial \tau^2} + \bar{I}_E\frac{\partial^2 \Psi}{\partial \tau^2},\end{aligned} \tag{24a}$$

$$\begin{aligned}&\eta\frac{\partial^2 U}{\partial X^2}\frac{\partial W}{\partial X} + \bar{B}_{11}\eta\frac{\partial^2 \Theta}{\partial X^2}\frac{\partial W}{\partial X} + \frac{3}{2}\eta^2\left(\frac{\partial W}{\partial X}\right)^2\frac{\partial^2 W}{\partial X^2} + \bar{E}_{11}\eta\frac{\partial^2 \Psi}{\partial X^2}\frac{\partial W}{\partial X} - M_{31}\eta\frac{\partial^2 W}{\partial X\,\partial \tau}\frac{\partial W}{\partial X}\\ &+\eta\frac{\partial U}{\partial X}\frac{\partial^2 W}{\partial X^2} + \bar{B}_{11}\eta\frac{\partial \Theta}{\partial X}\frac{\partial^2 W}{\partial X^2} + \bar{E}_{11}\eta\frac{\partial \Psi}{\partial X}\frac{\partial^2 W}{\partial X^2} - \bar{A}_{11}^T\Delta T\frac{\partial^2 W}{\partial X^2} - M_{31}\eta\frac{\partial W}{\partial \tau}\frac{\partial^2 W}{\partial X^2}\\ &+\bar{A}_{13}\left(\frac{1}{\eta}\frac{\partial \Theta}{\partial X} + \frac{\partial^2 W}{\partial X^2}\right) + \frac{\bar{B}_{13}}{\eta}\frac{\partial \Psi}{\partial X} + \frac{1}{4}\bar{A}_{13}l_0^2\eta\left(\frac{\partial^3 \Theta}{\partial X^3} - \eta\frac{\partial^4 W}{\partial X^4}\right) + \frac{1}{4}\bar{B}_{13}l_0^2\eta\frac{\partial^3 \Psi}{\partial X^3} - 2\bar{V}_x\frac{\partial^2 W}{\partial \tau \partial X}\\ &-\bar{V}_x^2\frac{\partial^2 W}{\partial X^2} + F_0F(X)T(\tau) - K_wW + K_g\frac{\partial^2 W}{\partial X^2} - K_c\frac{\partial W}{\partial \tau} - P\frac{\partial^2 W}{\partial X^2} = \frac{\partial^2 W}{\partial \tau^2},\end{aligned} \tag{24b}$$

$$\begin{aligned}&\frac{1}{4}\bar{A}_{13}l_0^2\left(\frac{\partial^2 \Theta}{\partial X^2} - \eta\frac{\partial^3 W}{\partial X^3}\right) + \frac{1}{4}\bar{B}_{13}l_0^2\frac{\partial^2 \Psi}{\partial X^2} - \frac{\bar{A}_{13}}{\eta}\left(\frac{1}{\eta}\Theta + \frac{\partial W}{\partial X}\right) - \frac{\bar{B}_{13}}{\eta^2}\Psi + \bar{B}_{11}\frac{\partial^2 U}{\partial X^2} + \bar{D}_{11}\frac{\partial^2 \Theta}{\partial X^2}\\ &+\bar{B}_{11}\eta\frac{\partial W}{\partial X}\frac{\partial^2 W}{\partial X^2} + \bar{F}_{11}\frac{\partial^2 \Psi}{\partial X^2} - 2\bar{I}_D\bar{V}_x\frac{\partial^2 \Theta}{\partial \tau \partial X} - \bar{I}_D\bar{V}_x^2\frac{\partial^2 \Theta}{\partial X^2} - 2\bar{I}_B\bar{V}_x\frac{\partial^2 U}{\partial \tau \partial X} - \bar{I}_B\bar{V}_x^2\frac{\partial^2 U}{\partial X^2}\\ &-2\bar{I}_F\bar{V}_x\frac{\partial^2 \Psi}{\partial \tau \partial X} - \bar{I}_F\bar{V}_x^2\frac{\partial^2 \Psi}{\partial X^2} = \bar{I}_B\frac{\partial^2 U}{\partial \tau^2} + \bar{I}_D\frac{\partial^2 \Theta}{\partial \tau^2} + \bar{I}_F\frac{\partial^2 \Psi}{\partial \tau^2},\end{aligned} \tag{24c}$$

$$\bar{E}_{11}\frac{\partial^2 U}{\partial X^2}+\bar{F}_{11}\frac{\partial^2 \Theta}{\partial X^2}+\bar{E}_{11}\eta\frac{\partial W}{\partial X}\frac{\partial^2 W}{\partial X^2}+\bar{H}_{11}\frac{\partial^2 \Psi}{\partial X^2}-M_{32}\frac{\partial^2 W}{\partial X\,\partial\tau}-\frac{\bar{B}_{13}}{\eta}\left(\frac{\Theta}{\eta}+\frac{\partial W}{\partial X}\right)-\frac{\bar{D}_{13}}{\eta^2}\Psi$$
$$+\frac{1}{4}\bar{B}_{13}l_0^2\left(\frac{\partial^2\Theta}{\partial X^2}-\eta\frac{\partial^3 W}{\partial X^3}\right)+\frac{1}{4}\bar{D}_{13}l_0^2\frac{\partial^2\Psi}{\partial X^2}-\frac{1}{4}\bar{E}_{13}l_0^2\Psi-2\bar{I}_H\bar{V}_x\frac{\partial^2\Psi}{\partial\tau\partial X}-\bar{I}_H\bar{V}_x^2\frac{\partial^2\Psi}{\partial X^2} \quad (24d)$$
$$-2\bar{I}_E\bar{V}_x\frac{\partial^2 U}{\partial\tau\partial X}-\bar{I}_E\bar{V}_x^2\frac{\partial^2 U}{\partial X^2}-2\bar{I}_F\bar{V}_x\frac{\partial^2\Theta}{\partial\tau\partial X}-\bar{I}_F\bar{V}_x^2\frac{\partial^2\Theta}{\partial X^2}=I_E\frac{\partial^2 U}{\partial\tau^2}+I_F\frac{\partial^2\Theta}{\partial\tau^2}+I_H\frac{\partial^2\Psi}{\partial\tau^2},$$

and the dimensionless CC end conditions are obtained as follows:

$$U=0, W=0, \frac{\partial W}{\partial X}=0, \Theta=0, \Psi=0. \quad (25)$$

It is worth mentioning that the initial displacements and the initial velocities of the beam are assumed to be zero [55]. The dimensionless parameters used in Eqs. (24) and (25) are defined as:

$$(U,W)=\left(\frac{u}{h_l},\frac{w}{h_l}\right),\Theta=\theta,\Psi=\psi,l_0=\frac{l}{h_l},X=\frac{x}{L},\eta=\frac{h_l}{L},\Gamma=\gamma,\tau=\frac{t}{L}\sqrt{\frac{A_{11}}{I_A}},\Omega=\omega L\sqrt{\frac{I_A}{A_{11}}},$$
$$\left(\bar{B}_{11},\bar{E}_{11},\bar{D}_{11},\bar{F}_{11},\bar{H}_{11}\right)=\left(\frac{B_{11}}{A_{11}h_l},\frac{E_{11}}{A_{11}h_l},\frac{D_{11}}{A_{11}h_l^2},\frac{F_{11}}{A_{11}h_l^2},\frac{H_{11}}{A_{11}h_l^2}\right),M_{31}=\frac{2bh_L e_{31}k_c c(t)}{\sqrt{I_A A_{11}}},$$
$$M_{32}=\frac{E_{31}k_c c(t)}{h\sqrt{I_A A_{11}}},\left(\bar{A}_{11}^T,\bar{B}_{11}^T,\bar{E}_{11}^T\right)=\left(\frac{A_{11}^T}{A_{11}},\frac{B_{11}^T}{A_{11}h_l},\frac{E_{11}^T}{A_{11}h_l}\right), \quad (26)$$
$$\left(\bar{I}_B,\bar{I}_E,\bar{I}_D,\bar{I}_F,\bar{I}_H\right)=\left(\frac{I_B}{I_A h_l},\frac{I_E}{I_A h_l},\frac{I_D}{I_A h_l^2},\frac{I_F}{I_A h_l^2},\frac{I_H}{I_A h_l^2}\right),K_c=\frac{k_c L}{\sqrt{I_A A_{11}}},K_w=\frac{k_w L^2}{A_{11}},K_g=\frac{k_g}{A_{11}},$$
$$\left(\bar{A}_{13},\bar{B}_{13},\bar{D}_{13},\bar{E}_{13}\right)=\left(\frac{A_{13}}{A_{11}},\frac{B_{13}}{A_{11}},\frac{D_{13}}{A_{11}},\frac{E_{13}L^2}{A_{11}}\right),F_0=\frac{f_0 L^2}{A_{11}h_l},\bar{V}_x=V_x\sqrt{\frac{I_A}{A_{11}}},P=\frac{p}{A_{11}},$$

In which:

$$\left(A_{11},B_{11},D_{11}\right)=\sum_{k=1}^{3}\int_{A_k}Q_{11}^k\left\{1,z,z^2\right\}dA_k,\left(E_{11},F_{11},H_{11}\right)=\sum_{k=1}^{3}\int_{A_k}Q_{11}^k\Phi^{(k)}(z)\left\{1,z,\Phi^{(k)}(z)\right\}dA_k, \quad (27a)$$

$$E_{31}=\int_{-h_l/2}^{-h_c/2}e_{31}\Phi(z)bdz+\int_{h_c/2}^{h_l/2}e_{31}\Phi(z)bdz, \quad (27b)$$

$$\left(A_{13},B_{13},D_{13},E_{13}\right)=\sum_{k=1}^{3}\int_{A_k}Q_{55}^k\left\{1,\Phi^{(k)}{}_{,z}(z),\left[\Phi^{(k)}{}_{,z}(z)\right]^2,\left[\Phi^{(k)}{}_{,zz}(z)\right]^2\right\}dA_k \quad (27c)$$

$$\left(A_{11}^T,B_{11}^T\right)=\sum_{k=1}^{3}\int_{A_k}Q_{11}^k\alpha_x^k\left\{1,z\right\}dA_k,E_{11}^T=\sum_{k=1}^{3}\int_{A_k}Q_{11}^k\alpha_x^k\Phi^{(k)}(z)dA_k, \quad (27d)$$

6 NUMERICAL SOLUTION

The DQM which used in the present manuscript to discretize the space domain is a numerical method that predicts the derivative of a function at a given discrete point as a weighted linear sum of the function values at all discrete points chosen in the solution domain. Even though the DQM is a numerical result but it yields accurate results and

can be chosen as an effective method to solve the governing motion equations. At first, the positions of the grid point in space domain can be obtained using Chebyshev polynomials as follows [19, 27, 28]:

$$X_n = \frac{1}{2}\left(1-\cos\left(\frac{\pi(n-1)}{N-1}\right)\right), \quad n=1,2,\ldots,N \tag{28}$$

where N is the total number of grid points along X. Also, the functions U, W, Θ and Ψ and their r *th* derivatives with respect to X can be expressed as [19, 27, 28]:

$$\{U,W,\Theta,\Psi\} = \sum_{m=1}^{N} l_m(X)\{U_m(X_m,\tau), W_m(X_m,\tau), \Theta_m(X_m,\tau), \Psi_m(X_m,\tau)\}, \tag{29a}$$

$$\frac{\partial^r}{\partial X^r}\{U,W,\Theta,\Psi\}\Big|_{X=X_n} = \sum_{m=1}^{N} C_{nm}^{(r)}(X)\{U_m(X_m,\tau), W_m(X_m,\tau), \Theta_m(X_m,\tau), \Psi_m(X_m,\tau)\}, \tag{29b}$$

In which $l_m(X)$ and $C_{nm}^{(k)}$ are the Lagrange interpolation polynomials and the weighting coefficients, which can be found in [20, 21, 23]. Substituting Eqs. (29) into Eqs. (24) and (25) yields:

$$\begin{aligned}
&\sum_{m=1}^{N} C_{nm}^{(2)} U_m + \bar{B}_{11}\sum_{m=1}^{N} C_{nm}^{(2)}\Theta_m + \eta\sum_{m=1}^{N} C_{nm}^{(1)} W_m \sum_{m=1}^{N} C_{nm}^{(2)} W_m + \bar{E}_{11}\sum_{m=1}^{N} C_{nm}^{(2)}\Psi_m - M_{31}\sum_{m=1}^{N} C_{nm}^{(1)}\ddot{W}_m \\
&-2\bar{V}_x\sum_{m=1}^{N} C_{nm}^{(1)}\dot{U}_m - \bar{V}_x^2\sum_{m=1}^{N} C_{nm}^{(2)} U_m - 2\bar{I}_B\bar{V}_x\sum_{m=1}^{N} C_{nm}^{(1)}\dot{\Theta}_m - \bar{I}_B\bar{V}_x^2\sum_{m=1}^{N} C_{nm}^{(2)}\Theta_m - 2\bar{I}_E\bar{V}_x\sum_{m=1}^{N} C_{nm}^{(1)}\dot{\Psi}_m \\
&-\bar{I}_E\bar{V}_x^2\sum_{m=1}^{N} C_{nm}^{(2)}\Psi_m = \ddot{U}_n + \bar{I}_B\ddot{\Theta}_n + \bar{I}_E\ddot{\Psi}_n,
\end{aligned} \tag{30a}$$

$$\begin{aligned}
&\eta\sum_{m=1}^{N} C_{nm}^{(2)} U_m \sum_{m=1}^{N} C_{nm}^{(1)} W_m + \bar{B}_{11}\eta\sum_{m=1}^{N} C_{nm}^{(2)}\Theta_m \sum_{m=1}^{N} C_{nm}^{(1)} W_m + \frac{3}{2}\eta^2\left(\sum_{m=1}^{N} C_{nm}^{(1)} W_m\right)^2 \sum_{m=1}^{N} C_{nm}^{(2)} W_m \\
&+\bar{E}_{11}\eta\sum_{m=1}^{N} C_{nm}^{(2)}\Psi_m \sum_{m=1}^{N} C_{nm}^{(1)} W_m - M_{31}\eta\sum_{m=1}^{N} C_{nm}^{(1)}\ddot{W}_m \sum_{m=1}^{N} C_{nm}^{(1)} W_m + \eta\sum_{m=1}^{N} C_{nm}^{(1)} U_m \sum_{m=1}^{N} C_{nm}^{(2)} W_m \\
&+\bar{B}_{11}\eta\sum_{m=1}^{N} C_{nm}^{(1)}\Theta_m \sum_{m=1}^{N} C_{nm}^{(2)} W_m + \bar{E}_{11}\eta\sum_{m=1}^{N} C_{nm}^{(1)}\Psi_m \sum_{m=1}^{N} C_{nm}^{(2)} W_m - \bar{A}_{11}^{T}\Delta T\sum_{m=1}^{N} C_{nm}^{(2)} W_m \\
&-M_{31}\eta\ddot{W}_n\sum_{m=1}^{N} C_{nm}^{(2)} W_m + \bar{A}_{13}\left(\frac{1}{\eta}\sum_{m=1}^{N} C_{nm}^{(1)}\Theta_m + \sum_{m=1}^{N} C_{nm}^{(2)} W_m\right) + \frac{\bar{B}_{13}}{\eta}\sum_{m=1}^{N} C_{nm}^{(1)}\Psi_m \\
&+\frac{1}{4}\bar{A}_{13} l_0^2\eta\left(\sum_{m=1}^{N} C_{nm}^{(3)}\Theta_m - \eta\sum_{m=1}^{N} C_{nm}^{(3)} W_m\right) + \frac{1}{4}\bar{B}_{13} l_0^2\eta\sum_{m=1}^{N} C_{nm}^{(3)}\Psi_m - 2\bar{V}_x\sum_{m=1}^{N} C_{nm}^{(1)}\dot{W}_m \\
&-\bar{V}_x^2\sum_{m=1}^{N} C_{nm}^{(2)} W_m + F_0 F(X_n)T(T) - K_w W_n + K_g\sum_{m=1}^{N} C_{nm}^{(2)} W_m - K_c\dot{W}_n - P\sum_{m=1}^{N} C_{nm}^{(2)} W_m = \ddot{W}_n,
\end{aligned} \tag{30b}$$

$$\begin{aligned}
&\frac{1}{4}\bar{A}_{13} l_0^2\left(\sum_{m=1}^{N} C_{nm}^{(2)}\Theta_m - \eta\sum_{m=1}^{N} C_{nm}^{(3)} W_m\right) + \frac{1}{4}\bar{B}_{13} l_0^2\sum_{m=1}^{N} C_{nm}^{(2)}\Psi_m - \frac{\bar{A}_{13}}{\eta}\left(\frac{1}{\eta}\Theta_n + \sum_{m=1}^{N} C_{nm}^{(1)} W_m\right) - \frac{\bar{B}_{13}}{\eta^2}\Psi_n \\
&+\bar{B}_{11}\sum_{m=1}^{N} C_{nm}^{(2)} U_m + \bar{D}_{11}\sum_{m=1}^{N} C_{nm}^{(2)}\Theta_m + \bar{B}_{11}\eta\sum_{m=1}^{N} C_{nm}^{(1)} W_m \sum_{m=1}^{N} C_{nm}^{(2)} W_m + \bar{F}_{11}\sum_{m=1}^{N} C_{nm}^{(2)}\Psi_m - 2\bar{I}_D\bar{V}_x\sum_{m=1}^{N} C_{nm}^{(1)}\dot{\Theta}_m \\
&-\bar{I}_D\bar{V}_x^2\sum_{m=1}^{N} C_{nm}^{(2)}\Theta_m - 2\bar{I}_B\bar{V}_x\sum_{m=1}^{N} C_{nm}^{(1)}\dot{U}_m - \bar{I}_B\bar{V}_x^2\sum_{m=1}^{N} C_{nm}^{(2)} U_m - 2\bar{I}_F\bar{V}_x\sum_{m=1}^{N} C_{nm}^{(1)}\dot{\Psi}_m - \bar{I}_F\bar{V}_x^2\sum_{m=1}^{N} C_{nm}^{(2)}\Psi_m \\
&= \bar{I}_B\ddot{U}_n + \bar{I}_D\ddot{\Theta}_n + \bar{I}_F\ddot{\Psi}_n,
\end{aligned} \tag{30c}$$

$$\begin{aligned}
&\bar{E}_{11}\sum_{m=1}^{N}C_{nm}^{(2)}U_m+\bar{F}_{11}\sum_{m=1}^{N}C_{nm}^{(2)}\Theta_m+\bar{E}_{11}\eta\sum_{m=1}^{N}C_{nm}^{(1)}W_m\sum_{m=1}^{N}C_{nm}^{(2)}W_m+\bar{H}_{11}\sum_{m=1}^{N}C_{nm}^{(2)}\Psi_m-M_{32}\sum_{m=1}^{N}C_{nm}^{(1)}\dot{W}_m\\
&-\frac{\bar{B}_{13}}{\eta}\left(\frac{\Theta_n}{\eta}+\sum_{m=1}^{N}C_{nm}^{(1)}W_m\right)-\frac{\bar{D}_{13}}{\eta^2}\Psi_n+\frac{1}{4}\bar{B}_{13}l_0^2\left(\sum_{m=1}^{N}C_{nm}^{(2)}\Theta_m-\eta\sum_{m=1}^{N}C_{nm}^{(3)}W_m\right)+\frac{1}{4}\bar{D}_{13}l_0^2\sum_{m=1}^{N}C_{nm}^{(2)}\Psi_m\\
&-\frac{1}{4}\bar{E}_{13}l_0^2\Psi_n--2\bar{I}_H\bar{V_x}\sum_{m=1}^{N}C_{nm}^{(1)}\dot{W}_m-\bar{I}_H\bar{V_x}^2\sum_{m=1}^{N}C_{nm}^{(2)}\Psi_m-2\bar{I}_E\bar{V_x}\sum_{m=1}^{N}C_{nm}^{(1)}\dot{U}_m-\bar{I}_E\bar{V_x}^2\sum_{m=1}^{N}C_{nm}^{(2)}U_m\\
&-2\bar{I}_F\bar{V_x}\sum_{m=1}^{N}C_{nm}^{(1)}\dot{\Theta}_m-\bar{I}_F\bar{V_x}^2\sum_{m=1}^{N}C_{nm}^{(2)}\Theta_m=\bar{I}_E\ddot{U}_n+\bar{I}_F\ddot{\Theta}_n+\bar{I}_H\ddot{\Psi}_n,
\end{aligned}\tag{30d}$$

The dot notation over the variables denotes the derivations of the mentioned variables to the time. Using Eqs. (29) yields the CC boundary conditions as follows:

$$U_1=0,W_1=0,\sum_{m=1}^{N}C_{1m}^{(1)}W_m=0,\Theta_1=0,\Psi_1=0,\tag{31a}$$

$$U_N=0,W_N=0,\sum_{m=1}^{N}C_{Nm}^{(1)}W_m=0,\Theta_N=0,\Psi_N=0,\tag{31b}$$

Considering Eqs. (30) and (31), one can rewrite governing motion equations as follows:

$$[M]\{\ddot{d}\}+[C_{NL}+C_L]\{\dot{d}\}+[K_{NL}+K_L]\{d\}=\{F\},\tag{32}$$

In which $[M]$ is the mass matrix, $[C_{NL}+C_L]$ are the nonlinear and linear damping matrixes, $[K_{NL}+K_L]$ are the nonlinear and linear stiffness matrixes and $\{F\}$ is the transverse load matrix and:

$$\{d\}=\left\{\{U_i\}^T,\{W_i\}^T,\{\Theta_i\}^T,\{\Psi_i\}^T\right\},\tag{33}$$

In the next step, the implicit time integration Newmark-β method [56] is employed to find the time response of the SNB. The algorithm of the Newmark-β method can be described as follows:

1) From Eq. (32) and primary conditions of time for displacements and velocities terms, the acceleration terms are obtained as:

$$\{\ddot{d}\}=[M]^{-1}\left(\{F\}-[C_{NL}+C_L]\{\dot{d}\}-[K_{NL}+K_L]\{d\}\right),\tag{34}$$

2) Choosing an appropriate time step Δt, and coefficients α and β the following parameters can be obtained:

$$a_0=\frac{1}{\beta(\Delta t)^2},a_1=\frac{\alpha}{\beta\Delta t},a_2=\frac{1}{\beta\Delta t},a_3=\frac{1}{2\beta}-1,a_4=\frac{\alpha}{\beta}-1,a_5=\frac{\Delta t}{2}\left(\frac{\alpha}{\beta}-2\right),\tag{35}$$

It is also worth mentioning that in the present manuscript $\alpha=\frac{1}{2}$ and $\beta=\frac{1}{4}$.

3) The effective stiffness matrix can be defined as follows:

$$[K]=[K_L+K_{NL}]+a_0[M]+a_1[C_L+C_{NL}],\tag{36}$$

4) For each time step the effective force vector can be calculated from those obtained from previous time step as follows:

$$\{F_{t+\Delta t}\}=\{F_{t+\Delta t}\}+[M]\left(a_0\{d_t\}+a_2\{\dot{d}_t\}+a_3\{\ddot{d}_t\}\right)+[C_L+C_{NL}]\left(a_1\{d_t\}+a_4\{\dot{d}_t\}+a_5\{\ddot{d}_t\}\right). \tag{37}$$

5) After that the displacement vector can be obtained from:

$$\{d_{t+\Delta t}\}=[K]^{-1}\{F_{t+\Delta t}\}. \tag{38}$$

6) Therefore, from Eq. (38), the following terms can be calculated as:

$$\begin{aligned}\{\dot{d}_{t+\Delta t}\}&=a_1\left(\{d_{t+\Delta t}\}-\{d_t\}\right)-a_4\{\dot{d}_t\}-a_5\{\ddot{d}_t\},\\ \{\ddot{d}_{t+\Delta t}\}&=a_0\left(\{d_{t+\Delta t}\}-\{d_t\}\right)-a_2\{\dot{d}_t\}-a_3\{\ddot{d}_t\}.\end{aligned} \tag{39}$$

7) For each time step the problem can be solved from step 4 and finally the time history can be obtained.

7 RESULTS AND DISCUSSIONS

The influences of small scale parameter, visco-Pasternak elastic foundation, magnetostrictive layers, temperature difference, environment temperature, velocity of SNB, applied mechanical loads and volume fraction exponent on the dynamic bending of the axially moving SNB subjected to transverse load $F_0e^{-a\tau}\sin(\pi X)(a=0.1)$ is presented in this section. To this purpose, the material properties of Terfenol-*D* which is chosen as the magnetostrictive material, are presented in Table 1.

Table 1
Material properties of magnetostrictive layers made of Terfenol-*D* [45].

Terfenol-*D*
$E=26.5(GPa)$
$d^m=1.67\times10^{-8}(m/A)$
$e_{31}=e_{32}=442.55(N/mA)$
$\rho_l=9250(Kg/m^3)$

Based on Eq. (23), the temperature coefficients of the FG core layer are reported in Table 2 based on the information presented in Pradhan [48].

Table 2
Material properties of the FGM core [48].

	Stainless Steel		Nickel	
Density (kg/m^3)	7900		8909	
Coefficient	E (N/m^2)	ν	E (N/m^2)	ν
P_0	201.04×10^9	0.3262	244.27×10^9	0.2882
P_{-1}	0	0	0	0
P_1	3.079×10^{-4}	2.002×10^{-4}	-1.371×10^{-4}	1.133×10^{-4}
P_2	-6.534×10^{-7}	3.797×10^{-7}	1.214×10^{-7}	0
P_3	0	0	-3.681×10^{-7}	0

In order to calculate the material properties of FG core layer, the environment temperature is assumed to be $T=25^{\circ}C$. Unless otherwise mentioned, results presented here are based on the following data: the core thickness $h_c=1(nm)$, the thickness of each magnetostrictive layer $h_m=0.25(nm)$,the aspect ratio of length to the thickness

$L/h_l = 8$, the small scale parameter $l = 0.2h_l$, the temperature difference $\Delta T = 0^{\circ}C$, the control gain value $k_c c(t) = 0$, the dimensionless velocity of the SNB $\bar{V}_x = 0.01$, volume fraction exponent of FG core layer $\gamma = 0$, the axial force $p = 0(N)$, the dimensionless constant of the distributed transverse load $F_0 = 0.5$, the spring constant of elastic medium $k_w = 100(MN/m^2)$, the shear constant of elastic medium $k_g = 1(nN)$ and the damping modulus constant of elastic foundation $k_c = 3\times10^{-4}(kg/ms)$.

7.1 Convergence and verification of the numerical results

First, in order to check the convergence and accuracy of the DQM, the appropriate number of grid points are obtained. For this purpose, the maximum dimensionless midpoint deflections ($W|_{X=0.5}$) of the SNB for different values of grid points for both linear and nonlinear analysis are presented in Table 3. As can be seen for $N = 15$ the maximum values of $W|_{X=0.5}$ are converged to 0.724 for linear and 0.634 for nonlinear analysis. Therefore, $N = 15$ is chosen to calculate the numerical results of the present manuscript.

Table 3
Maximum values of dimensionless midpoint deflection for different number of grid points.

Types of solution	N=5	N=7	N=9	N=11	N=13	N=15	N=17
Linear	0.498	0.689	0.710	0.719	0.722	0.724	0.724
Nonlinear	0.561	0.644	0.622	0.631	0.632	0.634	0.634

In order to check the validity of the obtained results, since no published paper is found on the nonlinear dynamic bending of an axially moving SNB, the results obtained from the presented numerical solutions are compared with those obtained from the exact solution in Fig. 2, by neglecting the axially moving, surrounding elastic medium, nonlinear terms, power law exponent of FG core layer and magnetostrictive layer effects for the Roller-Roller (RR) boundary conditions. It is seen from Fig. 2 that the results concluded from DQM in conjunction with the Newmark-β method are in good agreement with those obtained from the exact solutions. It is notable that the exact solutions used here to check the validity of the obtained results, include Navier method for space domain and Laplace transform for time domain. Moreover, neglecting the mentioned parameters, the dimensionless RR boundary conditions are expressed in Appendix A.

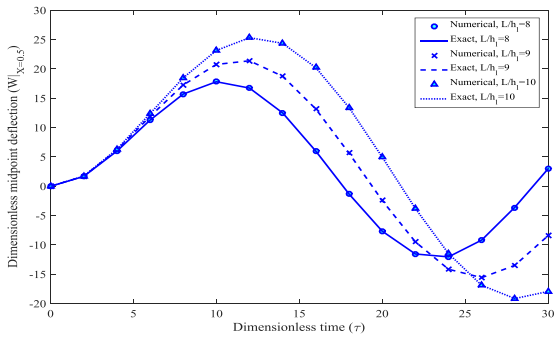

Fig.2
Verification of the results obtained by numerical solutions with those obtained by exact solutions.

7.2 Effect of different parameters

The effects of surrounding elastic medium on the dimensionless midpoint deflection of the axially moving SNB are illustrated in Figs. 3(a) and 3(b) for both linear and nonlinear analysis, respectively. Comparing Figs. 3(a) and 3(b) yields that the deflection of the SNB obtained from nonlinear analysis are lower than those obtained from linear solution. It is due to the fact that based on Eqs. (7a) and (9), considering nonlinear strain terms increases the strain energy and stiffness of the SNB and therefore, decreases the deflection of the system. From both Figs. 3(a) and 3(b), it is observed that considering elastic medium predicts lower deflection values than the results obtained without the elastic medium. Furthermore, it is seen from Figs. 3(a) and 3(b) that the Pasternak foundation predicts lower

deflection values than the Winkler medium, since Pasternak elastic foundation considers both spring and shear constants while Winkler medium considers only spring modulus. It is also worth mentioning that results obtained based on visco-Pasternak elastic medium are lower than those obtained by Pasternak foundation. As can be seen from Eq. (14), the visco-Pasternak elastic medium causes a damping term $k_c \dfrac{\partial w}{\partial t}$ in governing motion equation. The damping effect of this terms can be seen in both Figs. 3(a) and 3(b) where the visco-Pasternak elastic medium cause a reduction in dimensionless deflection as the time passes.

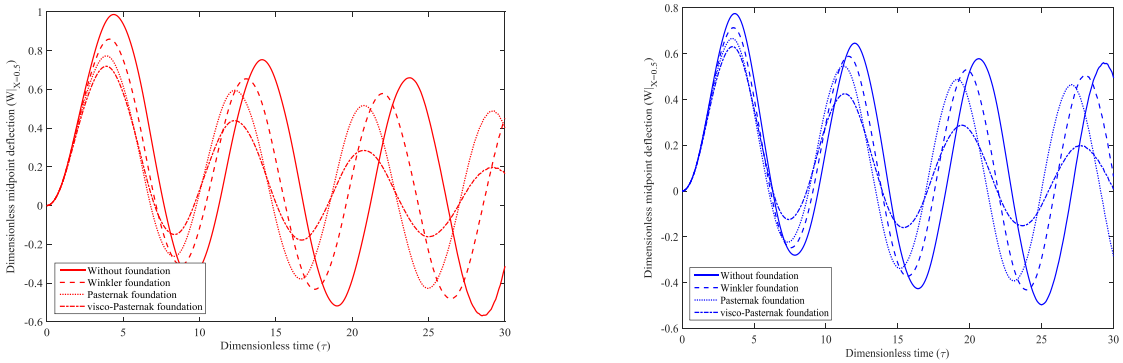

(a) (b)

Fig.3
Surrounding elastic foundation effects on the time history of dimensionless midpoint deflection of the SNB for a) Linear solution b) Nonlinear solution.

Figs. 4(a) and 4(b) show the material length scale parameter effects on the deflection of axially moving SNB for both linear and nonlinear solutions, respectively. It is seen from Fig. 4 that increasing material length scale parameter decreases the dynamic midpoint deflection of the system. Eqs. (1) and (20) prove this fact that increasing the small scale parameter, increases the strain energy of the SNB and therefore decreases the midpoint deflection. Moreover, the difference between linear and nonlinear results becomes more prominent at lower small scale parameter values. It is because that the difference between linear and nonlinear solutions becomes more visible in looser systems. Also, for linear or nonlinear analysis, the effect of small scale parameter is more distinguished at earlier times or in transient response region. In other words, with increasing the time the effect of material length scale parameter on the midpoint deflection of the system decreases.

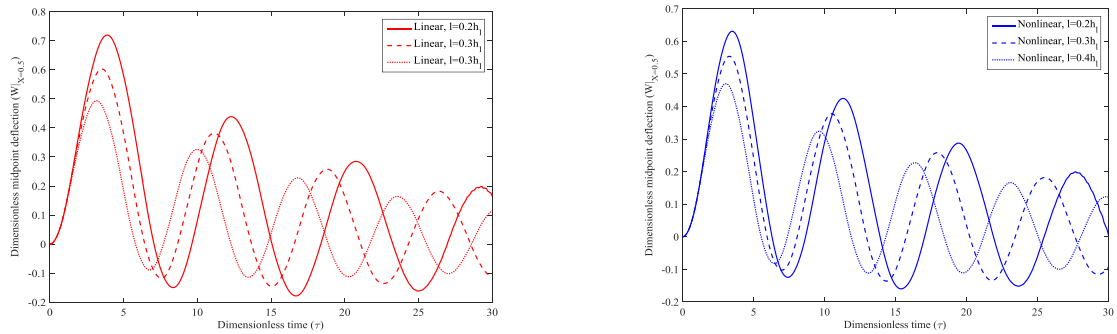

(a) (b)

Fig.4
Small scale effects on the time history of dimensionless midpoint deflection of the SNB for a) Linear solution b) Nonlinear solution.

To clarify the influences of external transverse load $F_0 e^{-a\tau} \sin(\pi X)$ on the midpoint deflection of the axially moving SNB, Figs. 5 and 6 are presented. Fig. 5 displays the variations of the distributed transverse load dimensionless constant versus dimensionless time. It is realized from Fig. 5 that increasing the dimensionless constant of the distributed transverse load cause to increases the midpoint deflection of the system. In addition, it is

worth to note that with increasing the distributed transverse load constant the difference between linear and nonlinear solutions decreases. Also, from Fig. 5, it is obtained that the effects of distributed transverse load constant are more prominent at transient response. In other words when the SNB reaches the steady state region the effect of the distributed transverse load constant decreases.

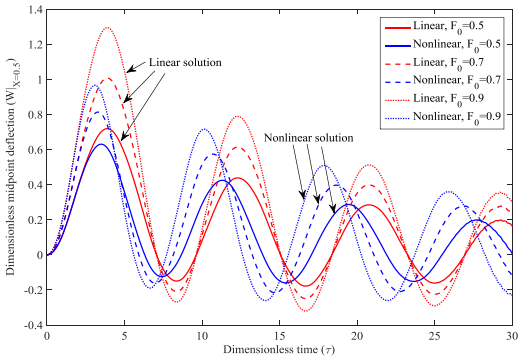

Fig.5
Dimensionless constant of distributed transverse load effects on the time history of dimensionless midpoint deflection of the SNB.

To investigate the effect of the parameter a in the transverse load on the dimensionless midpoint deflection of the SNB Figs. 6(a) and 6(b) are provided for linear and nonlinear solutions, respectively. It is clear that the parameter a is related to the damping ratio of the external transverse load. Therefore, with increasing this parameter, the transient response region should be decreased. This fact, can be easily seen in Fig. 6 in which increasing the parameter a reduces the transient response region of the SNB. Fig. 6 also shows that the linear and nonlinear solution differences become more prominent at lower values of the parameter a.

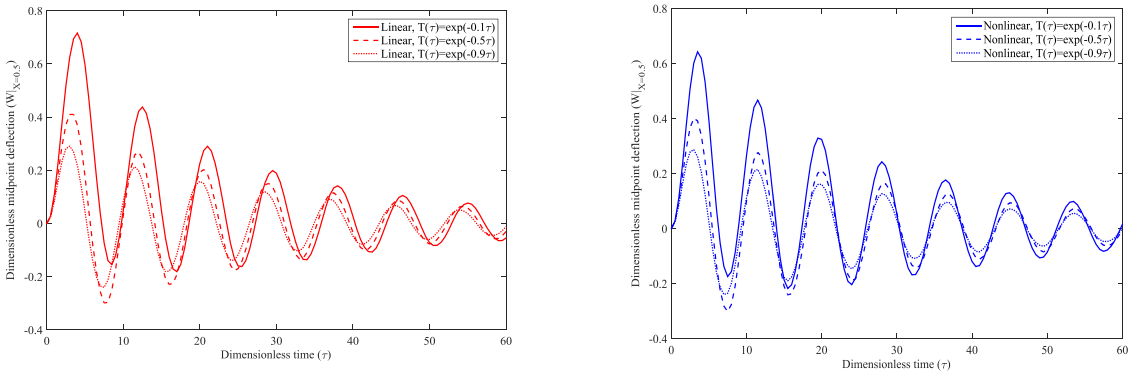

(a) (b)

Fig.6
Influence of the parameter a of transverse load on the time history of dimensionless midpoint deflection of the SNB for a) Linear solution b) Nonlinear solution.

In Fig. 7, the effects of temperature difference on the linear and nonlinear dynamic responses of CC axially moving SNB subjected to transverse load are examined. It is found from Fig. 7 that increasing the temperature difference, increases the midpoint deflection of the SNB. It is due to the fact that, according to Eqs. (1), (20a) and (20c), with increasing the temperature difference the stain energy of the system decreases, therefore the SNB midpoint deflection decreases. Furthermore, the effects of temperature difference becomes more obvious at steady state region for both linear and nonlinear analysis.

Time history of the dimensionless midpoint deflection of the CC axially moving SNB for linear and nonlinear solutions are illustrated in Fig. 8 for different values of temperature environments. The presented results in Fig. 8 reveal that as the temperature difference increases, the dimensionless midpoint deflection of the SNB increases, too. This result can also be theoretically obtained from Eqs. (1) and (20), in which increasing the temperature environment of the SNB, reduces the stresses and strain energy of the SNB, that yields increasing in midpoint deflection of the system.

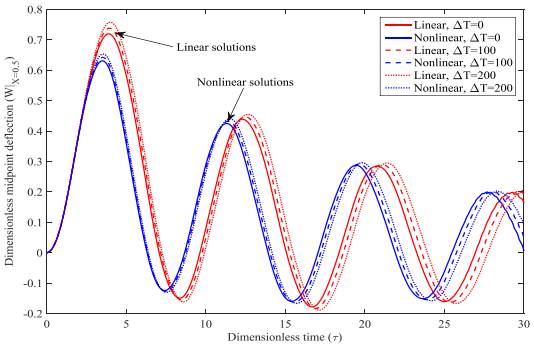

Fig.7
Temperature difference effect on the time history of dimensionless midpoint deflection of the SNB.

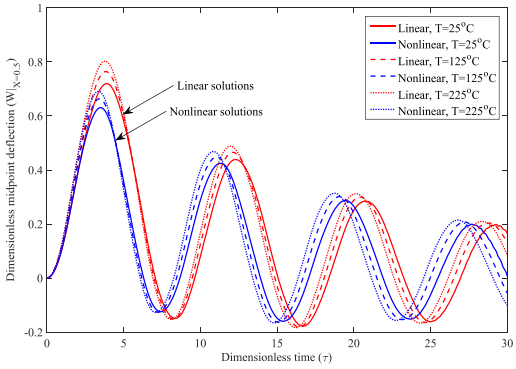

Fig.8
Environment temperature effect on the time history of dimensionless midpoint deflection of the SNB.

Fig. 9 indicates the SNB velocity effect on the maximum values of dimensionless midpoint deflection for both linear and nonlinear solutions and different values of volume fraction exponent. It is seen from Fig. 9 that increasing the velocity of increases the maximum deflection of SNB. Therefore, increasing the SNB velocity decreases the stability of the system. The obtained numerical results approve those obtained from physical investigations, where with increasing the velocity of systems, its stability decreases and therefore the deflection increases. Moreover, the difference between linear and nonlinear solutions becomes more prominent at higher velocity values. It is also worth mentioning that enhancing the volume fraction exponent values decreases the deflection of SNB. But it should be noted that increasing the volume fraction exponent values from 0 to 10 decreases the deflection at a decreasing rate. Therefore, one can conclude that increasing the volume of stainless steel in FG core decreases the deflection of system.

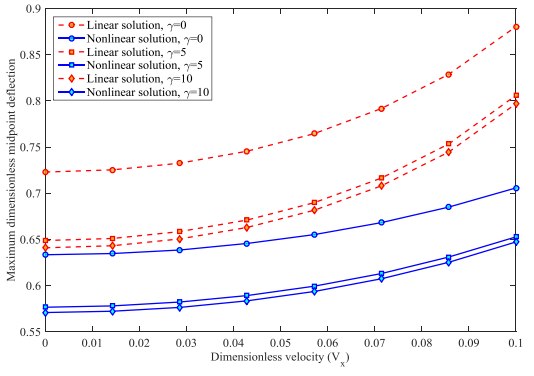

Fig.9
SNB velocity effect on the time history of maximum dimensionless midpoint deflection.

In order to show the effect of dimensionless axial load on the maximum dimensionless deflection of the SNB, Fig. 10 is plotted. As can be seen from Fig. 10, increasing the axial load yields an increase in maximum dimensionless deflection of SNB. This is because increasing the dimensionless axial load decreases the SNB stiffness and make the system looser. Similar to the velocity effect, the difference between linear and nonlinear solution enhances as the axial load increases. It is due to the fact that increasing the values of axial load, means that

the compressive axial load increases and the system stiffness decreases. Therefore, increasing the compressive axial load yields that the difference between linear and nonlinear solutions increases.

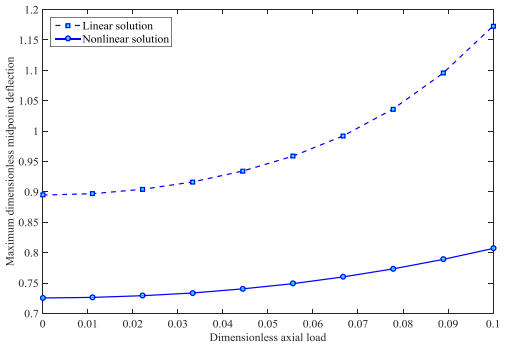

Fig.10
Axial load effect on the maximum values of dimensionless midpoint deflection.

The effects of magnetostrictive layers on the transient response of the SNB are shown on Figs. 11(a) and 11(b) by plotting the maximum dimensionless midpoint deflection versus velocity feedback gain ($k_c c(t)$) for both linear and nonlinear solutions, respectively. The obtained results show that increasing the velocity feedback gain from negative to positive values increases the maximum dimensionless midpoint deflection of the system. This result coincides with the mathematically point of view, where in Eq. (20c) and (21b) increasing the velocity feedback gain decreases the strain energy of the system and therefore, reduce the stability of the system. When the system loose its stability the deflection is increased. Hence, the velocity feedback gain can be used as a controller parameter and employing appropriate values for velocity feedback gain controls the dynamic response of the system. Furthermore, the linear solution in more sensitive to the axial load than nonlinear solution.

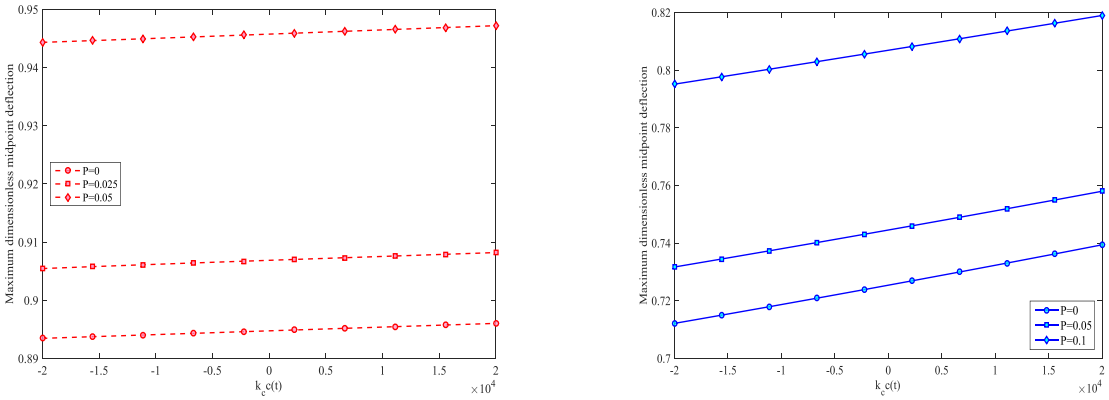

(a) (b)

Fig.11
Magnetostrictive layers effect on the time history of maximum dimensionless midpoint deflection a) Linear solution b) Nonlinear solution.

8 CONCLUSIONS

Geometrically nonlinear dynamic response of an axially moving FG Nano beam as the core layer integrated with a pair of magnetostrictive sensors embedded on visco-Pasternak elastic foundation under multi-physical loads was developed in this work. The temperature dependent material properties of FG core layer were assumed to vary along the thickness direction of the Nano beam. The MCST were utilized to capture the size effects on the dynamic response of the SNB. Applying energy method as well as Hamilton's principle, the governing motion equations were obtained. Both DQM and Newmark-β method were employed to find the dynamic response of the CC axially moving SNB. The obtained results by numerical method were compared with those obtained by the exact solution to certify the accuracy of the obtained results. Influences of surrounding elastic foundation, small scale parameter,

external transverse loads, temperature difference, environment temperature, magnetostrictive layers, velocity of the SNB, axial mechanical load, volume fraction exponent were investigated in details. The following conclusions can be outlined from the obtained results:

- It was concluded that the surrounding elastic medium has a significant effect on the dynamic response of the SNB. Using visco-Pasternak model reduces the midpoint deflection of the SNB.
- It was found that with increasing the material length scale parameter, the midpoint deflection of the SNB decreases. Therefore, the size effects cannot be neglected in nanostructure analysis.
- The difference between linear and nonlinear solutions becomes more pronounced when the transverse load constant increases.
- Increasing the velocity of SNB and also, axial load makes the system looser and therefore the maximum deflection increases.
- The maximum deflection of the SNB can be controlled and decreased using negative values for velocity feedback gain values.
- In order the decrease the maximum deflection of SNB, increasing the volume fraction exponent is suggested.

APPENDIX A

Considering Eqs. (19) and (26) the RR end conditions can be written as follows:

$$\sum_{m=1}^{N} C_{1m}^{(1)} U_m + \bar{B}_{11} \sum_{m=1}^{N} C_{1m}^{(1)} \Theta_m + \bar{E}_{11} \sum_{m=1}^{N} C_{1m}^{(1)} \Psi_m - \frac{\bar{A}_{11}^T \Delta T}{\eta} = 0, \tag{A.1}$$

$$W_1 = 0, \tag{A.2}$$

$$\bar{A}_{13} l_0^2 \left(\sum_{m=1}^{N} C_{1m}^{(1)} \Theta_m - \eta \sum_{m=1}^{N} C_{1m}^{(2)} W_m \right) + \bar{B}_{13} l_0^2 \sum_{m=1}^{N} C_{1m}^{(1)} \Psi_m = 0, \tag{A.3}$$

$$\begin{aligned} &\bar{B}_{11} \sum_{m=1}^{N} C_{1m}^{(1)} U_m + \bar{D}_{11} \sum_{m=1}^{N} C_{1m}^{(1)} \Theta_m + \frac{\bar{B}_{11}}{2} \eta \left(\sum_{m=1}^{N} C_{1m}^{(1)} W_m \right)^2 + \bar{F}_{11} \sum_{m=1}^{N} C_{1m}^{(1)} \Psi_m - \frac{\bar{B}_{11}^T}{\eta} \Delta T \\ &+ \frac{1}{4} \bar{A}_{13} l_0^2 \left(\sum_{m=1}^{N} C_{1m}^{(1)} \Theta_m - \eta \sum_{m=1}^{N} C_{1m}^{(2)} W_m \right) + \frac{1}{4} \bar{B}_{13} l_0^2 \sum_{m=1}^{N} C_{1m}^{(1)} \Psi_m = 0, \end{aligned} \tag{A.4}$$

$$\begin{aligned} &\bar{E}_{11} \sum_{m=1}^{N} C_{1m}^{(1)} U_m + \bar{F}_{11} \sum_{m=1}^{N} C_{1m}^{(1)} \Theta_m + \frac{\bar{E}_{11}}{2} \eta \left(\sum_{m=1}^{N} C_{1m}^{(1)} W_m \right)^2 + \bar{H}_{11} \sum_{m=1}^{N} C_{1m}^{(1)} \Psi_m - \frac{\bar{E}_{11}^T}{\eta} \Delta T \\ &+ \frac{1}{4} \bar{B}_{13} l_0^2 \left(\sum_{m=1}^{N} C_{1m}^{(1)} \Theta_m - \eta \sum_{m=1}^{N} C_{1m}^{(2)} W_m \right) + \frac{1}{4} \bar{D}_{13} l_0^2 \sum_{m=1}^{N} C_{1m}^{(1)} \Psi_m = 0, \end{aligned} \tag{A.5}$$

$$\sum_{m=1}^{N} C_{Nm}^{(1)} U_m + \bar{B}_{11} \sum_{m=1}^{N} C_{Nm}^{(1)} \Theta_m + \frac{\eta}{2} \left(\sum_{m=1}^{N} C_{Nm}^{(1)} W_m \right)^2 + \bar{E}_{11} \sum_{m=1}^{N} C_{Nm}^{(1)} \Psi_m - \frac{\bar{A}_{11}^T \Delta T}{\eta} = 0, \tag{A.6}$$

$$W_N = 0, \tag{A.7}$$

$$\bar{A}_{13} l_0^2 \left(\sum_{m=1}^{N} C_{Nm}^{(1)} \Theta_m - \eta \sum_{m=1}^{N} C_{Nm}^{(2)} W_m \right) + \bar{B}_{13} l_0^2 \sum_{m=1}^{N} C_{Nm}^{(1)} \Psi_m = 0, \tag{A.8}$$

$$\begin{aligned} &\bar{B}_{11} \sum_{m=1}^{N} C_{Nm}^{(1)} U_m + \bar{D}_{11} \sum_{m=1}^{N} C_{Nm}^{(1)} \Theta_m + \frac{\bar{B}_{11}}{2} \eta \left(\sum_{m=1}^{N} C_{Nm}^{(1)} W_m \right)^2 + \bar{F}_{11} \sum_{m=1}^{N} C_{Nm}^{(1)} \Psi_m - \frac{\bar{B}_{11}^T}{\eta} \Delta T \\ &+ \frac{1}{4} \bar{A}_{13} l_0^2 \left(\sum_{m=1}^{N} C_{Nm}^{(1)} \Theta_m - \eta \sum_{m=1}^{N} C_{Nm}^{(2)} W_m \right) + \frac{1}{4} \bar{B}_{13} l_0^2 \sum_{m=1}^{N} C_{Nm}^{(1)} \Psi_m = 0, \end{aligned} \tag{A.9}$$

$$\begin{aligned} &\bar{E}_{11} \sum_{m=1}^{N} C_{Nm}^{(1)} U_m + \bar{F}_{11} \sum_{m=1}^{N} C_{Nm}^{(1)} \Theta_m + \frac{\bar{E}_{11}}{2} \eta \left(\sum_{m=1}^{N} C_{Nm}^{(1)} W_m \right)^2 + \bar{H}_{11} \sum_{m=1}^{N} C_{Nm}^{(1)} \Psi_m - \frac{\bar{E}_{11}^T}{\eta} \Delta T \\ &+ \frac{1}{4} \bar{B}_{13} l_0^2 \left(\sum_{m=1}^{N} C_{Nm}^{(1)} \Theta_m - \eta \sum_{m=1}^{N} C_{Nm}^{(2)} W_m \right) + \frac{1}{4} \bar{D}_{13} l_0^2 \sum_{m=1}^{N} C_{Nm}^{(1)} \Psi_m = 0, \end{aligned} \tag{A.10}$$

REFERENCES

[1] Khedir A.A., Aldraihem O.J., 2016, Free vibration of sandwich beams with soft core, *Composite Structures* **154**: 179-189.

[2] Kahya V., 2016, Buckling analysis of laminated composite and sandwich beams by finite element method, *Composites Part B: Engineering* **91**: 126-134.

[3] Jedari Salami S., 2016, Dynamic extended high order sandwich panel theory for transient response of sandwich beams with carbon nanotube reinforced face sheets, *Aerospace Science and Technology* **56**: 56-69.

[4] Simsek M., Al-Shujairi M., 2017, Static, free and forced vibration of functionally graded (FG) sandwich beams excited by two successive moving harmonic loads, *Composites Part B: Engineering* **108**: 18-34.

[5] Kim N., Lee J., 2016, Theory of thin-walled functionally graded sandwich beams with single and double-cell sections, *Composite Structures* **157**: 141-154.

[6] Shi H., Liu W., Fang H., Bai Y., Hui D., 2017, Flexural responses and pseudo-ductile performance of lattice-web reinforced GFRP-wood sandwich beams, *Composites Part B: Engineering* **108**: 364-376.

[7] Arshid E., Khorshidvand A. R., 2018, Free vibration analysis of saturated porous FG circular plates integrated with piezoelectric actuators via differential quadrature method, *Thin-walled Structures* **125**: 220-233.

[8] Akgoz B., Civalek O., 2014, Mechanical analysis of isolated microtubules based on a higher-order shear deformation theory, *Composite Structures* **118**: 9-18.

[9] Ozutok A., Madenci E., 2017, Static analysis of laminated composite beams based on higher-order shear deformation theory by using mixed-type finite element method, *International Journal of Mechanical Sciences* **130**: 234-243.

[10] Shao D., Hu Sh., Wang Q., Pang F., 2017, Free vibration of refined higher-order shear deformation composite laminated beams with general boundary conditions, *Composites Part B: Engineering* **108**: 75-90.

[11] Zhang Zh., Taheri F., 2003, Dynamic pulsebuckling and postbuckling of composite laminated beam using higher order shear deformation theory, *Composites Part B: Engineering* **34**: 391-398.

[12] Altenbach H., Altenbach J., Kissing W., 2004, *Mechanics of Composite Structural Elements*, Springer.

[13] Tessler A., Di Sciuva M., Gherlone M., 2007, Refinement of Timoshenko beam theory for composite and sandwich beams using zigzag kinematics, Technical Report NASA/TP-2007-215086.

[14] Tessler A., Di Sciuva M., Gherlone M., 2009, A refined zigzag beam theory for composite and sandwich beams, *Journal of Composite Materials* **43**: 1051-1081.

[15] Nallim L.G., Oller S., Onate E., Flores F.G., 2017, A hierarchical finite element for composite laminated beams using a refined zigzag theory, *Composite Structures* **163**: 168-184.

[16] Di Sciuva M., Gherlone M., Iurlaro L., Tessler A., 2015, A class of higher-order C0 composite and sandwich beam elements based on the Refined Zigzag Theory, *Composite Structures* **132**: 784-803.

[17] Tessler A., Di Sciuva M., Gherlone M., 2010, A consistent refinement of first-order shear deformation theory for laminated composite and sandwich plates using improved zigzag kinematics, *Journal of Mechanics of Materials and Structures* **5**: 341-367.

[18] Gherlone M., Tessler A., Di Sciuva M., 2011, C0 beam elements based on the Refined Zigzag Theory for multilayered composite and sandwich laminates, *Composite Structures* **93**: 2882-2894.

[19] Abdollahian M., Ghorbanpour Arani A., Mosallaie Barzoki AA, Kolahchi R, Loghman A., 2013, Non-local wave propagation in embedded armchair TWBNNTs conveying viscous fluid using DQM, *Physica B* **418**: 1-15.
[20] Bagdatli S.M., 2015, Non-linear vibration of nanobeams with various boundary condition based on nonlocal elasticity theory, *Composites Part B: Engineering* **80**: 43-52.
[21] Aya S.A., Tufekci E., 2017, Modeling and analysis of out-of-plane behavior of curved nanobeams based on nonlocal elasticity, *Composites Part B: Engineering* **119**: 184-195.
[22] Ebrahiminejad S., Marzbanrad J., Boreiry M., Shaghaghi G. R., 2018, On the electro-thermo-mechanical vibration characteristics of elastically restrained functionally graded nanobeams using differential transformation method, *Applied Physics A* **124**: 800.
[23] Amir S., Khani A., Shajari A. R., Dashti P., 2017, Instability analysis of viscoelastic CNTs surrounded by a thermo-elastic foundation, *Structural Engineering & Mechanics* **63**: 171-180.
[24] Amir S., 2016, Orthotropic patterns of visco-Pasternak foundation in nonlocal vibration of orthotropic graphene sheet under thermo-magnetic fields based on new first-order shear deformation theory, *Proceedings of the Institution of Mechanical Engineers, Part L: Journal of Materials: Design and Applications*.
[25] Huang Y., Fu J., Liu A., 2019, Dynamic instability of Euler-Bernoulli nanobeams subject to parametric excitation, *Composites Part B: Enginerring* **164**: 226-234.
[26] Eringen A.C., 1983, On differential equations of nonlocal elasticity theory and solutions of screw dislocation and surface waves, *Journal of Applied Physics* **54**: 4703-4710.
[27] Ghorbanpour Arani A., Abdollahian M., Kolahchi R., 2015, Nonlinear vibration of embedded smart composite microtube conveying fluid based on modified couple stress theory, *Polymer Composites* **36**: 1314-1324.
[28] Ke L.L., Wang Y.Sh., 2011, Size effect on dynamic stability of functionally graded microbeams based on a modified couple stress theory, *Composite Structures* **93**: 342-350.
[29] Ke L.L., Wang Y.Sh., 2011, Flow-induced vibration and instability of embedded double-walled carbon nanotubes based on a modified couple stress theory, *Physica E: Low-dimensional Systemns and Nanostructures* **43**: 1031-1039.
[30] Ke L.L., Wang Y.Sh., Yang J., Kitipornchai S., 2012, Nonlinear free vibration of size-dependent functionally graded microbeams, International Journal of Engineering Science 50: 256-267.
[31] Ghayesh M.H., Farokhi H., Amabili M., 2013, Nonlinear dynamics of a microscale beam based on the modified couple stress theory, *Composites Part B: Engineering* **50**: 318-324.
[32] Ghorbanpour Arani A., Abdollahian M., Kolahchi R., 2015, Nonlinear vibration of a nanobeam elastically bonded with a piezoelectric nanobeam via strain gradient theory, *International Journal of Mechanical Sciences* **100**: 32-40.
[33] Akgoz B., Civalek O., 2011, Strain gradient elasticity theory and modified couple stress models for buckling analysis of axially loaded micro-scaled beams, *International Journal of Engineering Science* **49**: 1268-1280.
[34] Akgoz B., Civalek O., 2015, Bending analysis of FG microbeams resting on Winkler elastic foundation via strain gradient elasticity, *Composite Structures* **134**: 294-301.
[35] Hosseini M., Shishesaz M., Hadi A., 2019, Thermoelastic analysis of rotating functionally graded micro/nanodisks of variable thickness, *Thin-Walled Structures* **134**: 508-523.
[36] Dehghan M., Ebrahimi F., 2018, On wave dispersion characteristics of magneto-electro-elastic nanotubes considering the shell model based on the nonlocal strain gradient elasticity theory, *The European Physical Journal Plus* **133**:466.
[37] Amir S., Khorasani M., BabaAkbar-Zarei H., 2018, Buckling analysis of nanocomposite sandwich plates with piezoelectric face sheets based on flexoelectricity and first order shear deformation theory, *Journal of Sandwich Structures & Materials* **22**: 2186-2209.
[38] Amir S., Bidgoli E. M. R., Arshid E., 2018, Size-dependent vibration analysis of a three-layered porous rectangular nano plate with piezo-electromagnetic face sheets subjected to pre loads based on SSDT, *Mechanics of Advanced Materials and Structures* **27**: 605-619.
[39] Lee J.K., Jeong S., 2016, Flexural and torsional free vibrations of horizontally curved beams on Pasternak foundations, *Applied Mathematical Modelling* **40**: 2242-2256.
[40] Sobamowo M.G., 2017, Nonlinear thermal and flow-induced vibration analysis of fluid-conveying carbon nanotube resting on Winkler and Pasternak foundations, *Thermal Science and Engineering Progress* **4**: 133-149.
[41] Ghorbanpour Arani A., Abdollahian M., Kolahchi R., Rahmati A.H., 2013, Electro-thermo-torsional buckling of an embedded armchair DWBNNT using nonlocal shear deformable shell model, *Composites Part B: Engineering* **51**: 291-299.
[42] Liu J.C., Zhang Y.Q., Fan L.F., 2017, Nonlocal vibration and biaxial buckling of double-viscoelastic-FGM-nanoplate system with viscoelastic Pasternak medium in between, *Physics Letters A* **381**: 1228-1235.
[43] Mohammadi M., Safarabadi M., Rastgoo A., Farajpour A., 2016, Hygro-mechanical vibration analysis of a rotating viscoelastic nanobeam embedded in a visco-Pasternak elastic medium in a nonlinear thermal environment, *Acta Mechanica* **227**: 2207-2232.
[44] Jamalpoor A., Bahreman M., Hosseini M., Free transverse vibration analysis of orthotropic multi-viscoelastic microplate system embedded in visco-Pasternak medium via modified strain gradient theory, *Journal of Sandwich Structures & Materials* **21**: 175-210.
[45] Hong C.C., 2010, Transient responses of magnetostrictive plates by using the GDQ method, *European Journal of Mechanics A/Solid* **29**: 1015-1021.

[46] Hong C.C., 2014, Thermal vibration and transient response of magnetostrictive functionally graded material plates, *European Journal of Mechanics A/Solids* **43**: 78-88.
[47] Ghorbanpour Arani A., Abdollahian M., 2017, Transient response of FG higher order nanobeams integrated with magnetostrictive layers using modified couple stress theory, *Mechanics of Advanced Materials and Structures* **26**: 359-371.
[48] Pradhan S.C., 2005, Vibration suppression of FGM shells using embedded magnetostrictive layers, *International Journal of Solids and Structures* **42**: 2465-2488.
[49] Chang J.R., Lin W.J., Huang Ch.J., Choi S.T., 2010, Vibration and stability of an axially moving Rayleigh beam, *Applied Mathematical Modelling* **34**: 1482-1497.
[50] Ghayesh M.H., Amabili M., 2013, Steady-state transverse response of an axially moving beam with time-dependent axial speed, *International Journal of Non-Linear Mechanics* **49**: 40-49.
[51] Lim C.W., Li C., Yu J.L., 2010, Dynamic behavior of axially moving nanobeams based on nonlocal elasticity approach, *Acta Mechanica Sinica* **26**: 755-765.
[52] Rezaee M., Lotfan S., 2015, Non-linear nonlocal vibration and stability analysis of axially moving nanoscale beams with time-dependent velocity, *International Journal of Mechanical Sciences* **96-97**: 36-46.
[53] Ghorbanpour Arani A., Haghparast E., BabaAkbar Zarei H., 2016, Nonlocal vibration of axially moving grapheme sheet resting on orthotropic-Pasternak foundation under longitudinal magnetic field, *Physica B: Condensed Matter* **495**: 35-49.
[54] Ghorbanpour Arani A., Abdollahian M., Jalaei M.H., 2015, Vibration of bioliquid-filled microtubules embedded in cytoplasm including surface effects using modified couple stress theory, *Journal of Theoretical Biology* **367**: 29-38.
[55] Rao S.S., 2007, *Vibration of Continuous Systems*, John Wiley & Sons.
[56] Dukkipati, R.V., 2010, MATLAB: An Introduction with Applications, New Age International Publishers.